

IMPROVEMENT OF ELECTRICAL NEAR-FIELD MEASUREMENTS WITH AN ELECTRO-OPTIC TEST BENCH

D. Chevallier^{1,*}, D. Baudry², and A. Louis²

¹IRSEEM, EA 4353, Graduate School of Engineering ESIGELEC, Technopole du Madrillet, Av. Galilée, BP 10024, 76801 Saint Etienne du Rouvray Cedex, France

²CESI, 1 rue G. Marconi, Parc de la Vatine, 76130 Mont St Aignan, France

Abstract—In this paper, two different kinds of near-field measurement techniques are presented. The first one uses coaxial probes that do not give precise measurements on microelectronic devices. We saw in [1] that the spatial resolution of these probes reaches 500 μm for monopole and is millimetric for dipole probe. The second one is based on the Pockels effect that converts an electromagnetic (EM) field into optical modulation. Our objective is to improve the E_x/E_y near-field measurement with this second technique. The performance of the electro-optic (EO) probe is compared with dipole probes of 2.5 and 5 mm with the use of simulations and measurements, on a wire above a ground plane and on coupled microstrip lines. At the end, a discussion about the technical limitations of the EO probe is made.

1. INTRODUCTION

Measuring electric or magnetic field emitted by microelectronic components is a part of EMC research and near field modeling [2–4]. Equivalent sources for electromagnetic circuits diagnostics and characterization can also be used to predict the field radiated by the device under test. The results obtained are then used in a simulation platform to help developers in their design by taking into account these EMC strains. It can also be used to detect EM sources, to predict the EM radiated field by the DUT and to evaluate the EMI (ElectroMagnetic Interference) with other devices [5, 6].

Received 1 February 2012, Accepted 28 April 2012, Scheduled 12 May 2012

* Corresponding author: David Chevallier (chevallier@esigelec.fr).

Unfortunately, most of the current measurement techniques cannot describe completely all the emission and the coupling of the new microelectronic devices such as system in package (SIP) and system on chip (SOC) where a rise in electromagnetic interference problems is observed due to the high level of integration. A lack of sensitivity, spatial resolution or a coupling phenomenon can explain these limitations.

One of the most important parameters for these probes is the spatial resolution. Our current test bench is not sufficient to characterize the electromagnetic radiation due to a lack of spatial resolution. The coaxial probes that we have developed for EMC applications have a spatial resolution of 500 μm for monopole and around 1 mm for dipole probes which do not give enough experimental data with microelectronic components [7–10]. The optical probes can reach a spatial resolution under 100 μm and thus suitable for measuring microelectronic devices [11–13]. As a result, to improve the performance of our current near field bench based on passive detection with coaxial probes, and to analyze these interferences, we are currently developing another near-field test bench using optical technology based on the Pockels effect. This EO linear effect corresponds to the modulation of an optical beam in a crystal thanks to an electrical field. For magnetic field, magneto-optic (MO) crystals are used according to the Faraday's law [14–16]. In the telecommunication domain, a known EM field is used to modulate an optical signal and then to transmit data into optical fibers. In our case, the field is unknown, thus we have to analyze the change of the optical beam in order to quantify the EM field.

In this paper, two different measurement techniques, using dipole probes and EO probes, are described. First, different measuring equipments of each set-up are presented. Second, a preliminary study of the intrusive effect of the probes is done with HFSS (High Frequency Structure Simulator from Ansoft [17]). Third, the parameters of the probes such as linearity, selectivity, spatial resolution are analyzed using a wire above a ground plane (WPG) as the test device. In most of the cases, a comparison is made between the two measurement techniques. Finally an interdigital circuit is used to get more complicated profile and also cartography.

2. DESCRIPTION OF THE NEAR FIELD EQUIPMENT

2.1. Near-field Measurement Setup

The main part of the setup is the translation robot that holds the probe and moves it over the DUT to complete 2D EM field measurements.

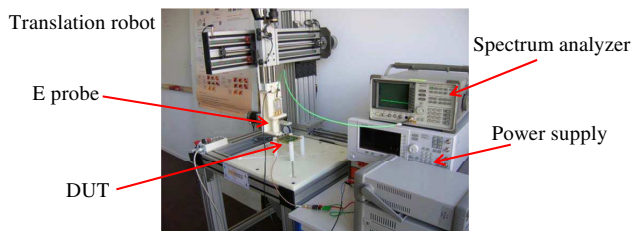


Figure 1. Equipment of the electrical near-field measurement setup.

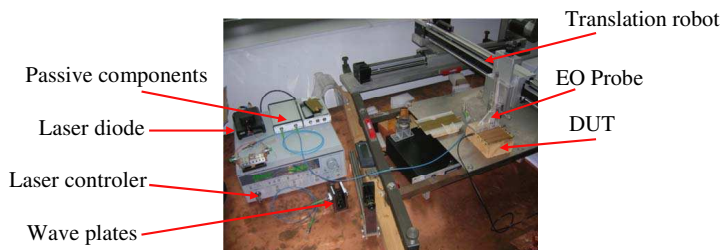


Figure 2. Equipment of the optical near-field measurement setup and mechanical support of the EO probe.

Fig. 1 shows a picture of one of the robot developed in Irseem with a mechanical resolution of $10\ \mu\text{m}$ in the 3 axes (x, y, z). A network or spectrum analyzer is used for detection. Fig. 2 represents the optical near-field measurement setup.

These systems allow us to perform repetitive measurements and also guarantee a safe utilization of the probes by controlling the distance probe/DUT. The second key equipment is the probe itself. To compare the performance of the two techniques, the dipole probes and the EO probe are presented. With the electrical bench and the dipole probes, the coupling between the radiation and the probe is measured by means of a network analyzer. With an optical near-field measurement setup based on polarization modulation, the rotation of light is measured to quantify the EM field [16, 18]. Figs. 3 and 4 show the schematics of the two test benches.

The optical near-field bench consists in a polarized laser source that injects a beam into a first polarizer. Then the signal reaches a circulator that leads the optical beam to the probes where the modulation occurs. Finally, the modulated signal goes back to the circulator and through a second polarizer and a 10 GHz photo detector. Inside the circulator, the light goes from port 1 to port 2 and next, from port 2 to port 3 it cannot go back to the laser (Isolation 60 dB).

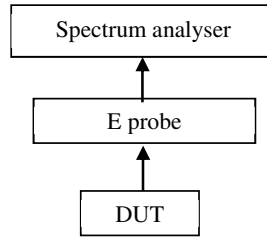


Figure 3. Measurement set-up of the electrical near-field bench.

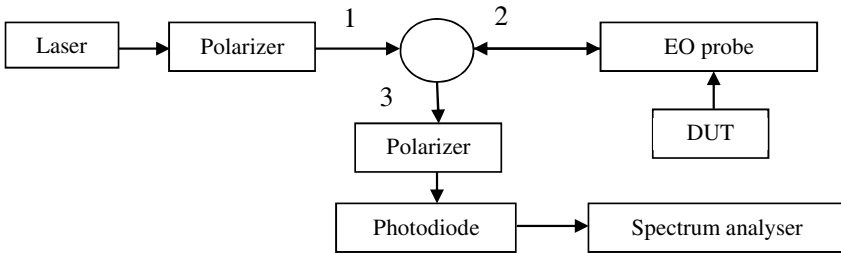


Figure 4. Measurement set-up of the optical near-field bench.

The intensity detected by the photodiode can be written as follows:

$$I = \frac{1}{2} \cos^2 \left(\frac{1}{2} \Gamma \right) \quad [19] \quad (1)$$

Γ represents the phase shift of the optical beam due to the modulation. This parameter is a function of the optical index of the crystal, its size, its Pockels coefficient and the magnitude of the EM field inside the crystal. To improve the setting, half and quarter wave plates can be added between the polarizer and the analyzer to precisely set the state of polarization of the incident beam to the crystal axes. The state of polarization is an ellipse; the aim of the setting is to adjust the axes of the ellipse with those of the optical fiber.

2.2. The Coaxial Probes

The electrical coaxial probes are fitted with one (Simple probe) or two (Differential probes) coaxial cables. These cables are composed of an inner and an outer conductor. The size of these conductors decides the performance of the probe, as the voltage V induced in a dipole by the incident field E is given by the following expression [7]:

$$V = - \int_{l/2}^{l/2} I(y) E(y) \quad (2)$$

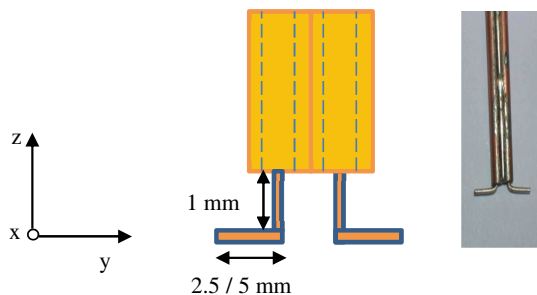


Figure 5. Schema of the E_x/E_y coaxial probes structure and picture of the 5 mm probe.

where l is the length of the dipole and I the current flowing in the probe.

However, the size is also linked to the probe's sensitivity, bringing us to a technical limit in the characterization of microelectronic components [7, 19, 20]. Fig. 5 shows a picture of our E_x/E_y dipole probes, fitted with 5 mm long conductors. A second version of this probe with 2.5 mm long conductors is used to discuss the influence of its size on the measurements. Finally, the coupling between the metallic parts of the probes and the field emitted by the DUT is analyzed.

2.3. The Structure of an EO Probe

The EO optical probes are made of a particular crystal. Each crystal has got specific parameters, creating a vectorial sensor able to measure a single or two components of an EM field [14, 15]. The crystal is fixed at the end of a polarization maintaining optical fiber, next to a GRIN lens which ensures the collimation of the light. It also has a high reflection (HR) coating at its bottom end to reflect back the optical beam into the optical fiber. Thus, the sensor can be used as a dipole probe on the near-field measurement setup. Fig. 6 presents the structure of an optical probe, and Fig. 7 shows its implementation and use with the near-field test bench.

To measure all the components of an EM field with optical technology, several probes would be needed but the optical bench will not change. The EO probe is developed by Kapteos [21] and is made of a LiTaO_3 cylinder crystal of 2*2 mm and designed to measure E_x/E_y electrical field component. This crystal has the same property of the well-known LiNbO_3 used in the optical modulator; its main advantage is its better Pockels coefficient. In the next part, the structure of the dipole probes is described.

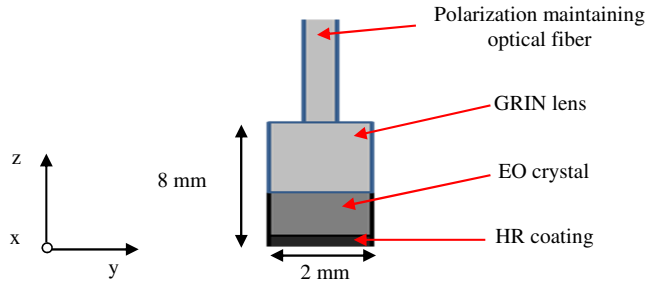


Figure 6. Structure of an optical probe.

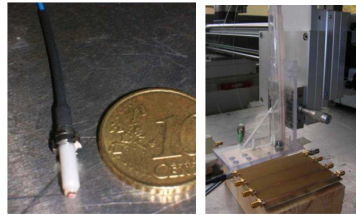


Figure 7. Picture of an EO probe and its implementation in the near-field measurement setup.

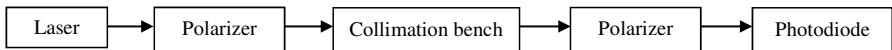


Figure 8. The crystal test bench set-up.

Now that structures of the probes are known, the analysis of their performance is presented below.

3. CHARACTERIZATION OF THE EO PROBE

Before testing the complete setting, each crystal can be analyzed on a transmission test bench.

3.1. Characterization of the Crystal

One major difficulty in the development of optical probes is to find a crystal of good quality. Before assembling the probes (which require some technical skill) it is important to test the response of the crystal on a transmission test bench (Figs. 8 and 9).

This is a collimation bench where any crystal can be fixed. It is placed in the optical near-field measurement setup instead of the

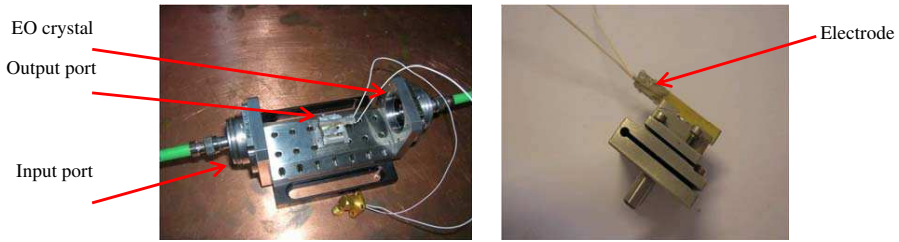


Figure 9. Elements of the collimation bench.

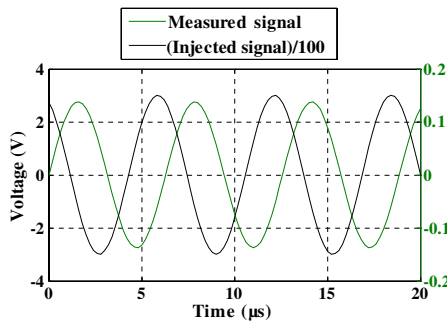


Figure 10. Analyze of the crystal on the collimation test bench.

circulator. The picture on the right of Fig. 9 shows a LiNbO_3 rectangular crystal on its mechanical support. Two electrodes are glued with silver lacquer so that a known electrical signal can be injected and measured. Fig. 10 shows the result obtained with this system at 130 kHz and 275 V. This injected signal is initially used to study EO modulator in practical work (Didaconcept [22]). A signal with a peak-to-peak voltage of 15 mV was measured. The electro-optic performances of any crystal can be analyzed with such a system. We can also change the length of the material sample to optimize the design of the micro optic assembly.

3.2. Intrusive Effect of the Probes

One other important step in the study of these probes is to know their influence on the measurement system. Electromagnetic simulations using HFSS are performed to qualify these influences [1]. In our subject, it is particularly interesting to compare this effect between the two technologies. To do so, the EM field is plotted on a 2D plane transverse to the microstrip line at 1 GHz. Fig. 11 represents the field lines emitted by the microstrip line without any probes. These field

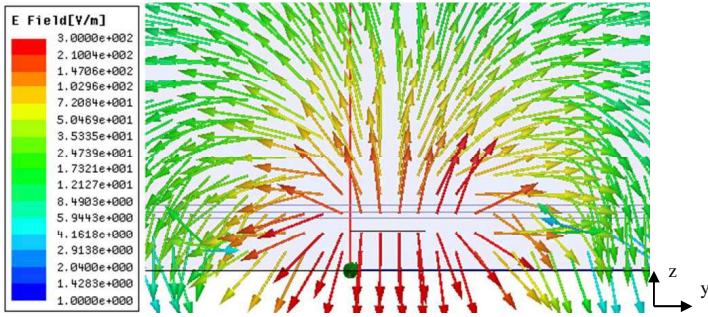


Figure 11. HFSS simulation at 1 GHz of the electrical field emitted by a microstrip line.

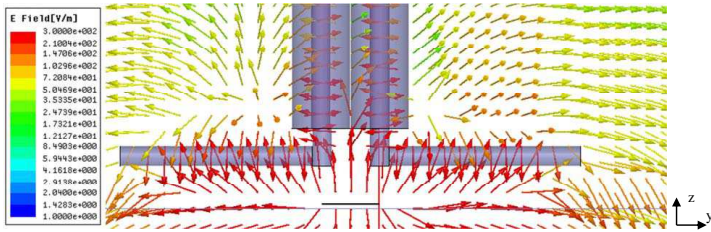


Figure 12. HFSS simulation at 1 GHz of the field lines in the presence of the dipole at $h = 1$ mm.

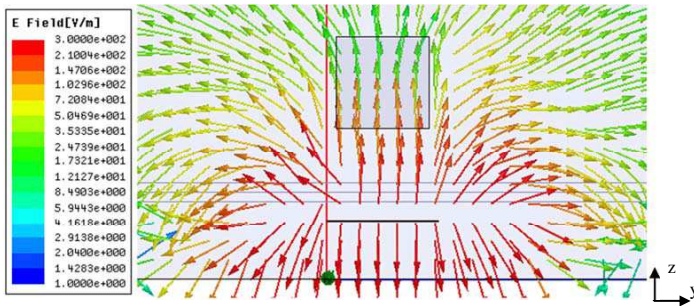


Figure 13. HFSS simulation at 1 GHz of the field lines in the presence of the EO crystal at $h = 1$ mm.

lines and the magnitude of the electric field are compared on Figs. 12 and 13 with those obtained with the probes.

First, the 5 mm dipole probe is introduced into the simulation. On the same plane, the EM field is plotted; the result obtained is shown in Fig. 12.

We see that the field magnitude does not decrease by the presence of the probe. However, the orientation of the field lines is affected. It is a representation of the coupling between the line and the coaxial cable. This coupling affects the quality of the measurement. Thus, the spatial resolution is directly affected by this phenomenon. Fig. 13 represents the same simulation with the EO probe instead of the dipole probes. In HFSS, the crystal is made from a high permittivity material (40.1). The EO crystal does not change the orientation of the field lines but the field inside the crystal decreases due to the high relative permittivity of the material ($\epsilon_r=40$).

The effect of the orientation of the field lines on the S parameters of the DUT with both probes can also be analyzed. Fig. 14 shows the effect of the presence of the EO probe and the dipole probe over a microstrip line on the S_{21} parameter. The differences between the curves with or without the probes are less than 1 dB.

3.3. Preliminary Characterization of the EO Probe

In the previous sections, we said that the Pockels effect was linear and the probe only sensitive to a particular component of an EM field. These two characteristics are the first ones to be quantified with each probe. For analyzing the linearity, the EO probe is placed above a microstrip line and the input power changed. The linearity was tested from 0 to 10 dBm at 10 MHz as shown in Fig. 15.

For the selectivity of the probe, two conducting plates fixed on a rotating platform were used (Fig. 16). The dipole and EO probe were placed between the two plates where an electrical signal was injected. Then, the field inside this structure was measured from 0° to 360° .

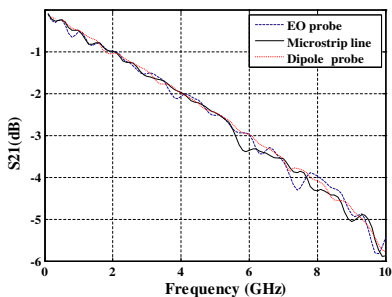


Figure 14. Intrusive effect of the EO probe and the dipole probe on the S_{21} .

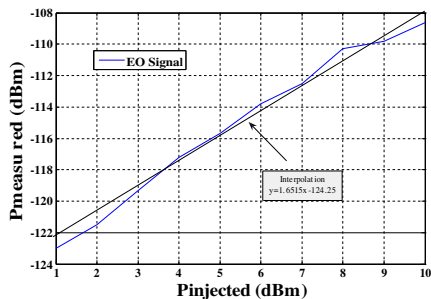


Figure 15. Linearity of the EO probe at 10 MHz, 1 mm above a microstrip line.

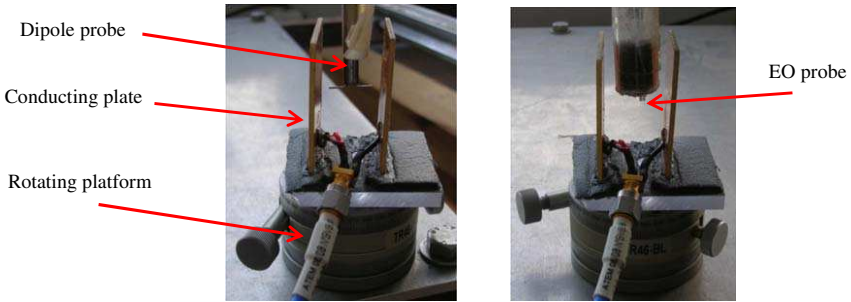


Figure 16. Conducting plates fixed on a rotating platform.

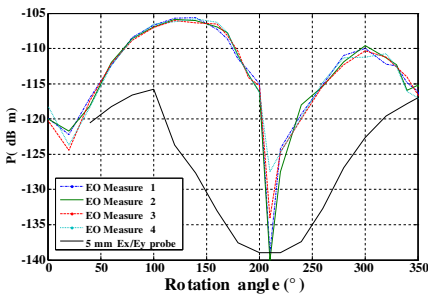


Figure 17. Selectivity of the dipole and the EO probe.



Figure 18. Rotation element fixed on the EO probe mechanical support.

Figure 17 shows the results of this test obtained with the two probes. Four measurements were made with the EO probe to show the repeatability of the technique. At 210° , we can see that the dipole response is far larger than the EO response.

This result is an illustration of the coupling effect of the dipole probes. The measurement of the E_y field is disturbed by the other E field components. The response of the EO probe is sharp; a proper orientation of this sensor above each DUT is then needed before conducting any other test, like measurements above a WGP. The rotating element shown in Fig. 18, with its precision of 2° can easily achieve this setting.

3.4. Characterization with a WGP

For this system, a comparison is made between the results obtained with the two technologies. Fig. 19 represents the placement of the probes in our measurements.

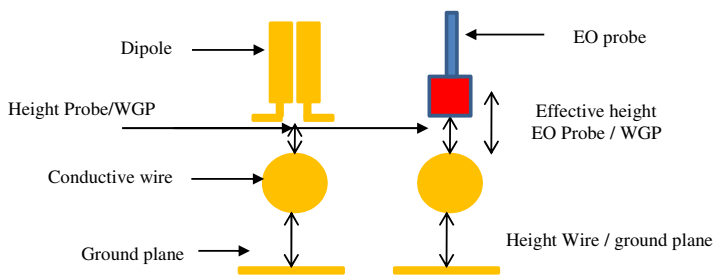


Figure 19. Setting of the measurements with the WGP.

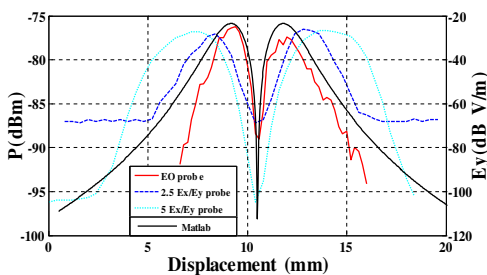


Figure 20. Comparison of the E_y field measured by the two dipoles, the EO probe and the analytic simulation at 10 MHz.

As the crystal’s size is affecting the effective measurements height, the EO probe needs to be closer to the DUT than the dipole probe. The dipole probe is placed 1 mm above the WGP and the EO probe 100 μm to get an effective height of 1 mm. These results are presented in Fig. 20. We can see that due to the coupling phenomenon, the dipole probes give larger profile. As the field is integrated along the length of the dipole, the 5 mm dipole has the larger profile. The EO curve is corresponding to the Matlab simulated profile at $h = 1$ mm.

The measured power is normalized in these curves; the maximum obtained with the dipole probes was -75 dBm and with the EO probe -103 dBm without any amplification system. These results really show that the optical near-field measurement setup has a big advantage against the coaxial probe. The absence of coupling with the crystal gives results corresponding to the real field emitted by the DUT. The EO probe also gives more local measurements due to the field integration along the dipole.

Nevertheless, the optical measurement bench has to be precisely fixed to have good sensitivity. Three wave plates can achieve this adjustment, without them, no cartography can be done as the

functioning point will be regularly lost [15]. The first wave plate ($\lambda/2$) is put between the circulator and the EO probe, the others (one $\lambda/4$ and one $\lambda/2$) are added before the second polarizer. In the next test presented in this article, coupled microstrip lines are used to analyze the spatial resolution of the EO probe.

3.5. Characterization with Coupled Lines

Coupled lines are conductive strips separated by a specific distance. The length of the gap between the lines is the same as their widths (200, 300, 500 and 700 μm). Fig. 21 represents the structure of the 200 μm coupled lines and a picture of the 4 coupled lines that we used.

With the help of HFSS simulations, the E_y field profile is obtained (300 μm coupled lines Fig. 22). This simulation was done at a height of 100 μm above the coupled lines. During our tests, the EO probe is placed at this height. We can note 4 maximums; the quantification of the spatial resolution consists in the ability of the probe to separate these peaks.

Figure 23 shows the transverse measurements realized with our EO probe above the 4 coupled lines. Even with the 700 μm coupled lines, only two peaks are measured.

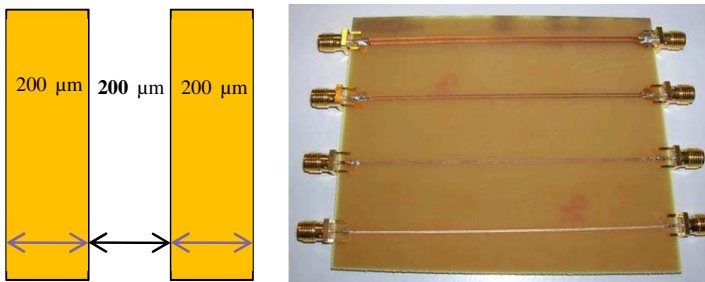


Figure 21. Schema and picture of the coupled lines.

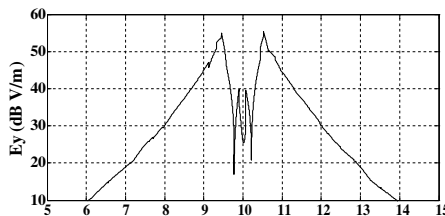


Figure 22. HFSS simulation of the E_y field emitted by 300 μm coupled lines at $h = 100 \mu\text{m}$ and $f = 10 \text{ MHz}$.

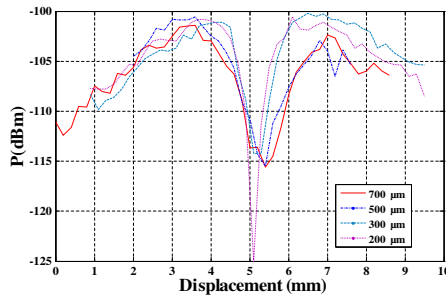


Figure 23. EO transverse measurement of the E_y field emitted by 100 to 700 μm coupled lines.

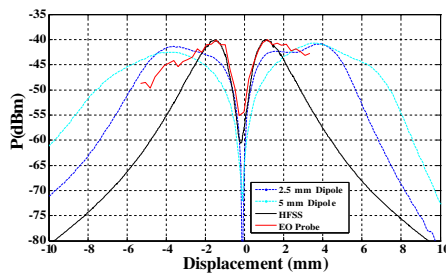


Figure 24. HFSS simulation of the E_y field emitted by 300 μm coupled lines at $h = 1$ mm and 10 MHz.

In Section 3.4, we saw that the size of the EO probe leads to measurements at a height of 1 mm when the probe is placed at 100 μm above the DUT. Fig. 24 shows the simulation and the measurements of the E_y field at a height of 1 mm with 300 μm coupled lines. Only two major peaks are present so we cannot conclude about the spatial resolution of the EO probe and the dipole probe in this configuration. The EO probe still keeps a profile closer to the simulation than the dipole. The distance between the DUT and the crystal needs to be reduced in order to detect the field that really characterizes the spatial resolution of the probe. While the optical bench is used for measurement, the optical beam traverses the EO crystal and thus the size of the laser beam inside the crystal determines the spatial resolution of the probe. The minimum resolution is fixed by the optical aperture of the optical fiber [15]. One solution consists in using a smaller crystal; M. Iwanami developed an ultra-small EO probe by depositing a PZT film onto an optical fiber edge using aerosol deposition [23]. With a better temperature control of the test bench and a dynamic adjustment of the polarization state of the laser beam,

thanks to the wave plates, the analyze of the spatial resolution of the EO probe would also be improved.

3.6. Characterization with Interdigital Circuit

Next to the study of the spatial resolution, the ability of the probe to analyze more complicated circuits is needed. An interdigital circuit is composed of 8 small microstrip lines (300 μm wide) each separated by 400 μm (Fig. 25).

With the help of HFSS, the E_y transverse field emitted by the interdigital circuit at 30 MHz is plotted (Fig. 26). We can see 6 maximums in this profile. With the same experimental protocol, this E_y field is measured and plotted Fig. 26.

The EO profile is almost the same as that in HFSS simulation. The two central maximums are not visible on the measurement curve. We saw on Section 3.5 that the EO probe, due to its size, presents a lack of spatial resolution. As a result, it cannot distinguish these two peaks separated by 400 μm . The EO probe is able to analyze the field of this interdigital circuit, but we can also see once again the necessity of improving the probe by reducing the crystal's size.

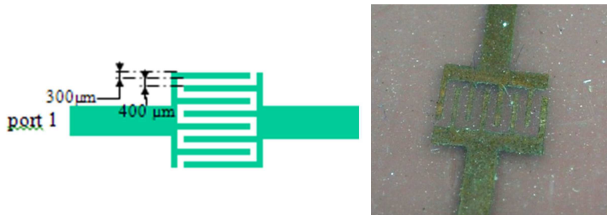


Figure 25. Schematic and picture of the interdigital circuit.

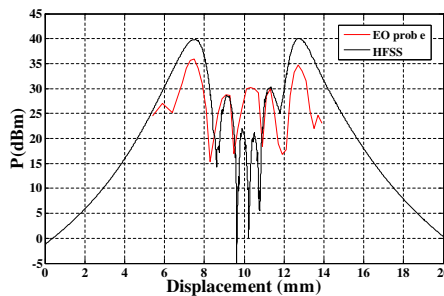


Figure 26. HFSS simulation and EO measurement of the E_y field emitted by the interdigital circuit at 30 MHz.

3.7. Practical Example Obtained with the EO Probe

This probe with its actual test bench is able to get good transverse measurement profile over DUT. However, the study of microelectronic components needs to be completed by cartography to have the vision of the device structure on the emitted field. The EO probe is fixed on the arm of the translation robot and moved over the microstrip line (Fig. 27) and the interdigital circuit (Fig. 28) to get their cartography.

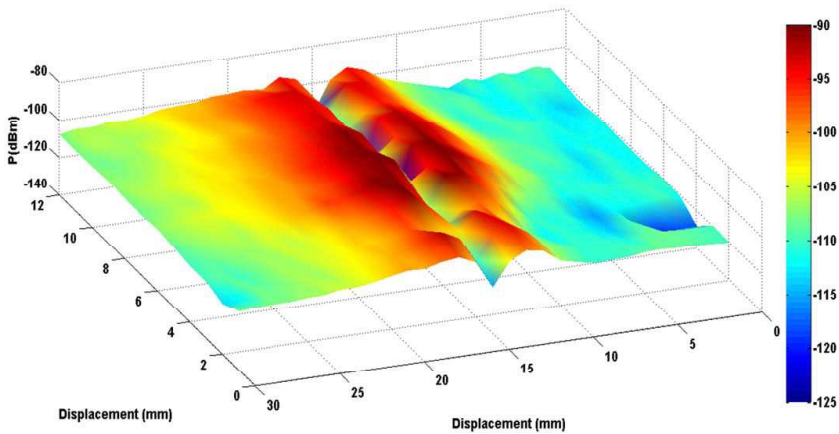


Figure 27. Cartography of the E_y field emitted by the microstrip line at $h = 1$ mm and 10 MHz.

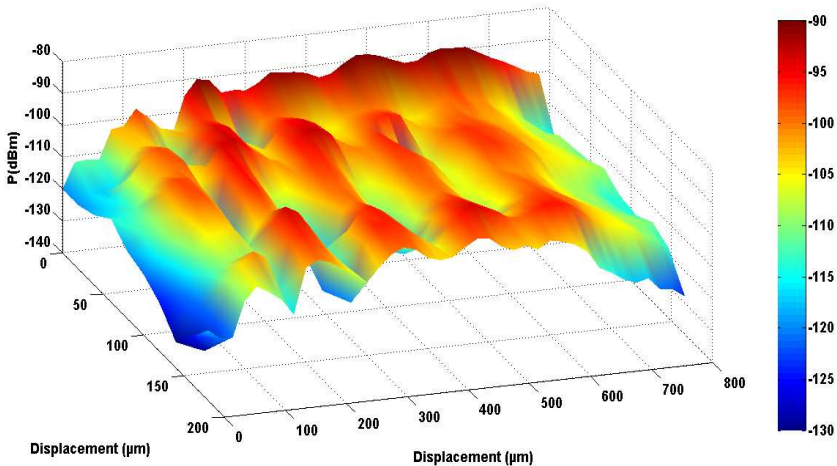


Figure 28. Cartography of the E_y field emitted by the interdigital circuit at $h = 1$ mm and 10 MHz.

These two results show that our test bench is able to carry out complete measurement over a DUT. With the help of cartographies, several details such as solder point or micro-connections should be visible on a more complicated circuit.

4. CONCLUSION

Two different near-field techniques that we used were presented in this paper. First, the test bench and two kinds of probes were described, and then several characterizations of the EO probe were done. We saw that the actual EO probe gives interesting results thanks to the absence of intrusive effect unlike the two dipole probes. However, the bench still needs to be improved to characterize the spatial resolution. In the near future, this setup will be placed in a clean room to limit the influence of temperature on the polarization state of the laser beam. A second probe with a smaller crystal would also give better results by reducing the distance between the DUT and the crystal. We plan to work with a MO crystal, Yttrium iron garnet (YIG), to detect the magnetic field radiations. These data will then be included in a neural network simulation tools to reduce the number of points needed for a near-field scan and to improve the spatial resolution [24].

ACKNOWLEDGMENT

These research works have been implemented within the frame of the MIST project which is funded by the Haute-Normandie Region (FRANCE).

REFERENCES

1. Chevallier, D., D. Baudry, A. Louis, and B. Mazari, "Study of near-field techniques for microelectronic applications," *Proc. Iconic*, 197–202, Taipei, Taiwan, Jun. 2009.
2. Baudry, D., C. Arcambal, A. Louis, B. Mazari, and P. Eudeline, "Applications of the near-field techniques in EMC applications," *IEEE Trans. on Electromagn. Compat.*, Vol. 49, 485–493, Aug. 2007.
3. Weng, H., D. G. Beetner, R. E. Dubroff, and J. Shi, "Estimation of high-frequency currents from near-field scan measurements," *IEEE Trans. on Electromagn. Compat.*, Vol. 49, No. 4, 805–815, Nov. 2007.

4. Vives, Y., C. Arcambal, A. Louis, F. de Daran, P. Eudeline, and B. Mazari, "Modeling magnetic radiations of electronic circuits using near-field scanning method," *IEEE Trans. on Electromagn. Compat.*, Vol. 49, No. 2, 391–399, May 2007.
5. Alvarez, Y., M. Rodriguez, F. Las-Heras, and M. M. Hernando, "On the use of the source reconstruction method for estimating radiated EMI in electronic circuits," *IEEE Transactions on Instrumentation and Measurement*, Vol. 49, No. 12, 3174–3183, Dec. 2010.
6. Hernando, M. M., A. Fernandez, M. Arias, M. Rodriguez, Y. Alvarez, and F. Las-Heras, "EMI radiated noise measurements using the sources reconstruction technique," *IEEE Transactions on Industrial Electronics*, Vol. 55, No. 9, 3258–3265, Sep. 2008.
7. Bouchelouk, L., Z. Riah, D. Baudry, M. Kadi, A. Louis, and B. Mazari, "Characterization of electromagnetic fields close to microwave devices using electric dipole probes," *International Journal of RF and Microwave Computer-aided Engineering*, Apr. 2007.
8. Baudry, D., A. Louis, and B. Mazari, "Characterization of the open-ended coaxial probe used for near-field measurements in EMC applications," *Progress In Electromagnetics Research*, Vol. 60, 311–333, 2006.
9. Manjombe, Y. T., Y. Azzouz, D. Baudry, B. Ravelo, and M. E. H. Benbouzid, "Experimental investigation on the power electronic transistor parameters influence to the near-field radiation for the EMC applications," *Progress In Electromagnetics Research M*, Vol. 21, 189–209, 2011.
10. Baudry, D., P. Fernandez-Lopez, B. Ejarque, N. Bigou, L. Bouchelouk, M. Ramdani, and S. Serpaud, "Near-field probes characterization and inter-laboratory comparisons of measurements," *Proc. EMC Compo*, Toulouse, Nov. 2009.
11. Yang, K., L. P. Katehi, and J. F. Whitaker, "Electric field mapping system using an optical-fiber based electrooptic probe," *IEEE Microwave and Wireless Components Letters*, Vol. 11, No. 4, Apr. 2001.
12. Yamazaki, E., S. Wakana, M. Kishi, and M. Tsuchiya, "Fabrication of broad-band fiber-optic magnetic field probe and its application to intensity and phase distribution measurements of GHz frequency magnetic field," *IEEE Microwave Photonics*, 77–80, Nov. 2002.
13. Whitaker, J. F., R. Reano, and P. B. Katehi, "Electro-optic field mapping as a diagnostic tool for microwave circuits and antenna

- arrays,” *Microwave Photonics*, 73–76, Nov. 2002.
14. Duvillaret, L., S. Rialland, and J. L. Coutaz, “Electro-optic sensors for electric field measurement. I. Theoretical comparison among different modulation techniques,” *J. Optic.*, Vol. 19, No. 11, Nov. 2002.
 15. Gaborit, G., “Caractérisation de champs électriques hyperfréquences par capteurs électro-optique vectoriels fibrés,” Doctorat de l’université de Savoie, Nov. 2005.
 16. Duvillaret, L., S. Rialland, and J. L. Coutaz, “Electro-optic sensors for electric field measurements. II. Choice of the crystals and complete optimization of their orientation,” *J. Optic Soc. Am. B*, Vol. 19, No. 11, Nov. 2002.
 17. <http://www.ansoft.com/products/hf/hfss/>.
 18. Togo, H., N. Shimizu, and T. Nagatsuma, “Near-field mapping system using fiber-based electro-optic probe for specific absorption rate measurement,” *IEICE Trans. on Electron.*, Vol. 90, No. 2, Feb. 2007.
 19. Gao, Y., A. Lauer, Q. Ren, and I. Wolff, “Calibration of electric coaxial near-field probes and applications,” *IEEE Transactions on Microwave Theory and Techniques*, Vol. 46, No. 11, 1694–1703, Nov. 1998.
 20. “IEEE standard for calibration of electromagnetic field sensors and probes, excluding antennas, from 9 kHz to 40 GHz,” IEEE Std., 1309–1346, 1996.
 21. <http://www.kapteos.com/fr/>.
 22. <http://didaconcept.free.fr/TP/TP%20MEO/Fiche%20EO.pdf>.
 23. Iwanami, M., M. Nakada, H. Tsuda, K. Ohashi, and J. Akedo, “Ultra small electro-optic field probe fabricated by aerosol deposition,” *IEICE Electronics Express*, Vol. 4, No. 2, 26–32,
 24. Brahimi, R., A. Komaga, M. Bensetti, D. Baudry, Z. Riah, and B. Mazari, “Post-processing of near-field measurement based on neural networks,” *IEEE Transactions on Instrumentation and Measurement*, Vol. 60, 539–546, Feb. 2011.